ANNUAL REVIEWS

Annual Review of Biochemistry

Driving E3 Ligase Substrate Specificity for Targeted Protein Degradation: Lessons from Nature and the Laboratory

Angus D. Cowan and Alessio Ciulli

Centre for Targeted Protein Degradation, School of Life Sciences, University of Dundee, Dundee, United Kingdom; email: a.ciulli@dundee.ac.uk

Annu. Rev. Biochem. 2022. 91:295–319

First published as a Review in Advance on March 23, 2022

The *Annual Review of Biochemistry* is online at biochem.annualreviews.org

https://doi.org/10.1146/annurev-biochem-032620-104421

Keywords

targeted protein degradation, E3 ligase, PROTAC, molecular glue, ubiquitin–proteasome system

Abstract

Methods to direct the degradation of protein targets with proximity-inducing molecules that coopt the cellular degradation machinery are advancing in leaps and bounds, and diverse modalities are emerging. The most used and well-studied approach is to hijack E3 ligases of the ubiquitin–proteasome system. E3 ligases use specific molecular recognition to determine which proteins in the cell are ubiquitinated and degraded. This review focuses on the structural determinants of E3 ligase recruitment of natural substrates and neo-substrates obtained through monovalent molecular glues and bivalent proteolysis-targeting chimeras. We use structures to illustrate the different types of substrate recognition and assess the basis for neo-protein–protein interactions in ternary complex structures. The emerging structural and mechanistic complexity is reflective of the diverse physiological roles of protein ubiquitination. This molecular insight is also guiding the application of structure-based design approaches to the development of new and existing degraders as chemical tools and therapeutics.

Contents

INTRODUCTION

Protein homeostasis in cells includes the many systems involved in maintaining a functional and dynamically responsive proteome. Along with protein synthesis, folding, and trafficking, molecular pathways that degrade proteins are essential for maintaining protein homeostasis. The ubiquitin–proteasome system (UPS) is one of the major pathways responsible for degrading intracellular protein targets. Through the UPS, proteins are tagged for degradation by ubiquitin, a small (8-kDa) protein that is highly conserved in eukaryotes. Three groups of enzymes are responsible for the priming and eventual ligation of ubiquitin to the substrate protein, primarily at a lysine residue. Ubiquitin is first activated in an ATP-dependent manner by an E1 enzyme, to which it becomes covalently attached. The E1 then transfers ubiquitin to an E2 enzyme via a *trans*-thiolation reaction. Finally, covalent ligation of the C terminus of ubiquitin to a lysine residue of a substrate protein is catalyzed by an E3 ligase (1, 2).

The mechanism of substrate ubiquitination differs among the various types of E3 ligases, including really interesting new gene (RING) E3s, homologous to E6-AP C terminus (HECT) E3s, and RING-between-RING (RBR) E3s (3, 4). The RING E3 ligases, most notably the Cullin–RING ligase (CRL) multi-subunit superfamily, bring the ubiquitin-loaded E2 and the target protein into close proximity for ubiquitin transfer directly from the E2 to the substrate (5, 6). HECT E3 ligases form a thioester intermediate with ubiquitin then subsequently transfer it to the substrate (7, 8). RBR E3 ligases use a hybrid of the RING and HECT E3 mechanisms, whereby the first RING domain binds to the E2, facilitating covalent transfer of ubiquitin to the second RING domain, followed by ubiquitin ligation to the substrate (9). In all cases, substrate specificity in the system is determined by the E3 ligase, which binds directly to the target substrate. Following the initial ubiquitination event, the substrate-linked ubiquitin can be ubiquitinated on one of several lysine residues, leading to the formation of polyubiquitin chains. Polyubiquitinated targets where ubiquitin molecules are linked at Lys48 or Lys63 are recognized by the proteasome, unfolded, and proteolytically degraded. Substrate recognition, ubiquitination, and degradation are presented schematically in **Figure 1*a***. Through the UPS, cells can rapidly respond to various stimuli to degrade or cease degradation of myriad proteins within the cell. In addition to linear chains, there are also branched ubiquitin chains that have recently been implicated in efficient signaling for proteasomal degradation (10, 11). Alternative types of ubiquitin chains beyond Lys48- and Lys63-linked chains can also be built by E3 ligases upon linkages to other lysine residues on ubiquitin (Lys6, Lys11, Lys27, Lys29, and Lys33) or to its N terminus (Met1) (12). These tend to have nondegrading roles, so they are not considered here.

Modulation and manipulation of the crucial role that the UPS plays within cells have been explored in recent years in both chemical biology and therapeutic contexts (13, 14). Redirection of

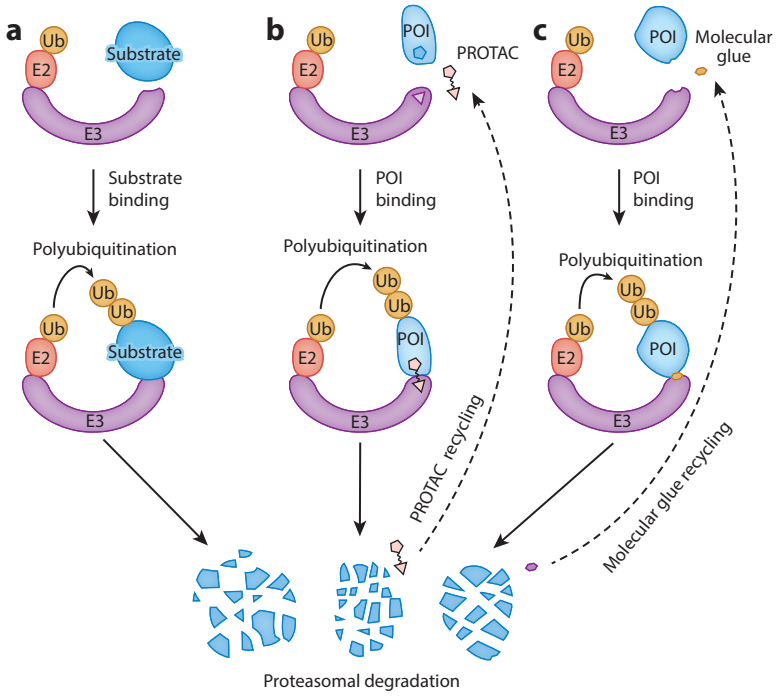

Figure 1

Native activity and pharmacological hijacking of E3 ligases. Graphical representation of (*a*) natural, (*b*) PROTAC-induced, and (*c*) molecular glue–induced protein degradation by the ubiquitin–proteasome system. Abbreviations: POI, protein of interest; PROTAC, proteolysis-targeting chimera; Ub, ubiquitin.

the ubiquitination machinery for targeted protein degradation (TPD) of nonnative neo-substrates is an emerging pharmacological strategy for disease intervention (15, 16). Early exploration of TPD by Howley and colleagues (17) involved fusing the human papillomavirus protein E7 and the CRL substrate receptor F-Box protein beta-transducin repeat containing protein (β-TrCP) with the object of eliminating the E7 binding partner retinoblastoma protein. The field of TPD blossomed further with the development of heterobifunctional peptidic molecules by the groups of Crews and Deshaies (18). In early proof-of-concept work, one end of the bifunctional molecule consisted of the natural peptide ligand for the β-TrCP E3 ligase substrate receptor and the other, the small molecule ovalicin, a ligand for methionine aminopeptidase (MetAP)-2 (18). These heterobifunctional molecules were termed proteolysis-targeting chimeras (PROTACs), and they bring the two proteins into proximity, leading to MetAP-2 ubiquitination and degradation in *Xenopus* egg extracts. The initial PROTACs were used only ex cellulo or required microinjection into cells. Subsequent work developed cell-permeable PROTACs consisting of a hypoxia-inducible factor 1-alpha (HIF1α) peptide to bind and recruit the E3 ligase CRL2 with its substrate receptor von Hippel-Lindau tumor suppressor protein (VHL) (with a polyarginine tag for cell permeability) fused to either an artificial ligand that binds mutant FKBP12 protein or a dihydrotestosterone derivative that binds the androgen receptor (19). Treatment of cells with these PROTACs led to TPD, highlighting the potential of such molecules as both biological tools and therapeutics. A decade later, nonpeptidic ligands for E3 ligases were developed, including for the CRL2 substrate receptor VHL and the CRL4 substrate receptor cereblon (CRBN). These ligands enabled the generation of much-improved PROTACs with potent and specific degradation activities that

are effective in cells and animal models (20–24). PROTACs have entered the clinic (25) almost two decades on from their pioneering introduction and are primed to deliver on their therapeutic promise. A schematic representation of the mechanism of action of a typical PROTAC is presented in **Figure 1*b***.

Two components determine substrate specificity for the ubiquitination of natural and non-natural substrates of E3 ligases. First, the substrate must contain a motif that can be recognized and engaged by the E3, and second, a lysine residue to which ubiquitin can be attached must be present and accessible to the E3 on the substrate. These two essential elements collectively represent a degron: the minimal recognition motif required to target a protein for degradation by the UPS. This review focuses on the first component, the molecular recognition of substrate and neo-substrate motifs by E3 ligases, in nature and in the context of chemical/pharmacological approaches to TPD, respectively. Examples are provided where the structural determinants are known. This review does not discuss fusion protein– and antibody-based TPD systems, which have been expertly reviewed elsewhere (26, 27).

Substrate ubiquitination and degradation must be dynamic to respond quickly to diverse intracellular and extracellular stimuli. Here, we broadly divide E3 binding and recognition of substrate degrons into three distinct types:

- **Type 1.** Recognition of a constitutive degron in the native fold of the substrate by a natively folded E3 ligase.
- **Type 2.** Recognition of a degron that arises from posttranslational modification (PTM) of the substrate.
- **Type 3.** Recognition of a substrate degron as a result of PTM of the E3 ligase.

Type 2 and 3 modifications can be further divided into interfacial or allosteric modifications and may be covalent or noncovalent or may involve a proteolytic cleavage event. A schematic representation of type 1, type 2, and type 3 substrate recognition is presented in **Figure 2**. General modifications that regulate E3 ligase function, such as neddylation of CRLs, and other types of substrate recognition, such as regulation by substrate receptor localization, have been reviewed recently (28) and are not discussed here.

Many hundreds of E3 ligases recognize myriad diverse substrate proteins, sometimes a single protein and sometimes whole families with conserved structural features. The molecular determinants of recognition have been investigated through structural methods, primarily by X-ray crystallography but increasingly by cryo–electron microscopy (cryo-EM). The next section discusses protein structures that have provided insights into the recognition process.

SUBSTRATE RECOGNITION IN NATURE

In type 1 substrate recognition, substrates may be constitutively degraded until inhibitory feedback mechanisms are engaged. Such is the case for the degradation of Dishevelled proteins (DVL)1–3, where the E3 ligase complex containing the BTB family Kelch-like protein 12 (KLHL12) as a substrate receptor, $CRL3^{KLHL12}$, constitutively recognizes and ubiquitinates DVL1–3 (29). Inhibition of $CRL3^{KLHL12}$ by NRX and PLEKHA4 allows the progression of Wnt signaling (30, 31). X-ray crystal structures of the CRL3 substrate receptor KLHL12 in complex with different DVL substrate peptides were reported recently by two groups (32, 33). The DVL1 structure revealed that the proline-rich PGXPP recognition motif in the peptide bound to the hydrophobic pocket at the center of the Kelch β-propeller adopts a U-shaped type II β-turn (34). The turn is stabilized by an intramolecular hydrogen bond between the backbone carbonyl of Pro657 and the backbone amine of Gly660 (residues *i* and *i*+3 in β-turn nomenclature,

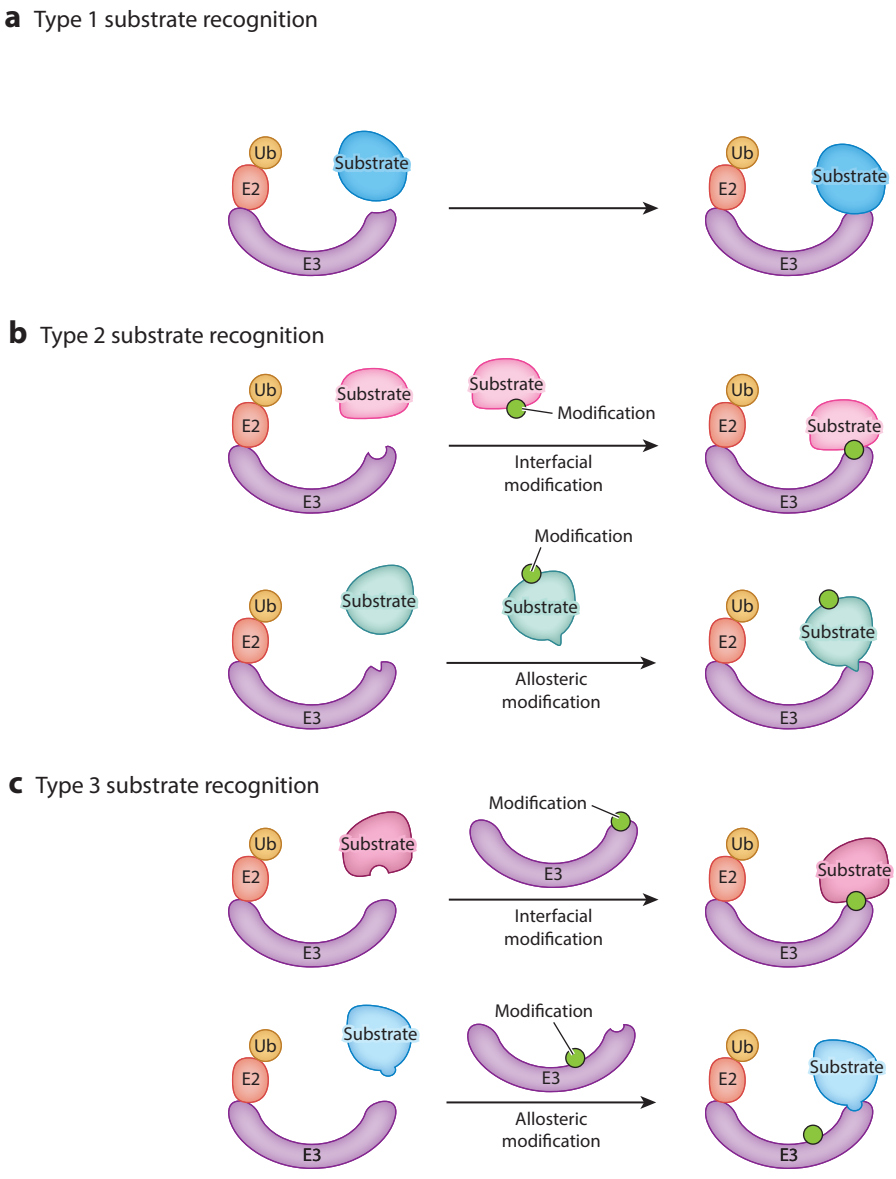

Figure 2

Types of substrate recognition by E3 ligases. Graphical representation of type 1, type 2, and type 3 substrate recognition. Modification of either the substrate (type 2) or the E3 ligase (type 3) may be either allosteric or interfacial. The modification may be covalent, noncovalent, or a proteolytic cleavage event. Abbreviation: Ub, ubiquitin.

respectively) (**Figure 3*a***). Bulky hydrophobic side chains in the KLHL12 barrel interact with the pyrrolidine rings of proline residues Pro658, Pro657, and Pro661 in the DVL1 peptide, and an intermolecular hydrogen bond is formed between the backbone carbonyl of Pro658 in DVL1 and the hydroxyl group of Tyr512 in KLHL12 (**Figure 3*a***). Other structurally characterized examples of type I substrate recognition can be found in the X-ray crystal structures of the CRL3

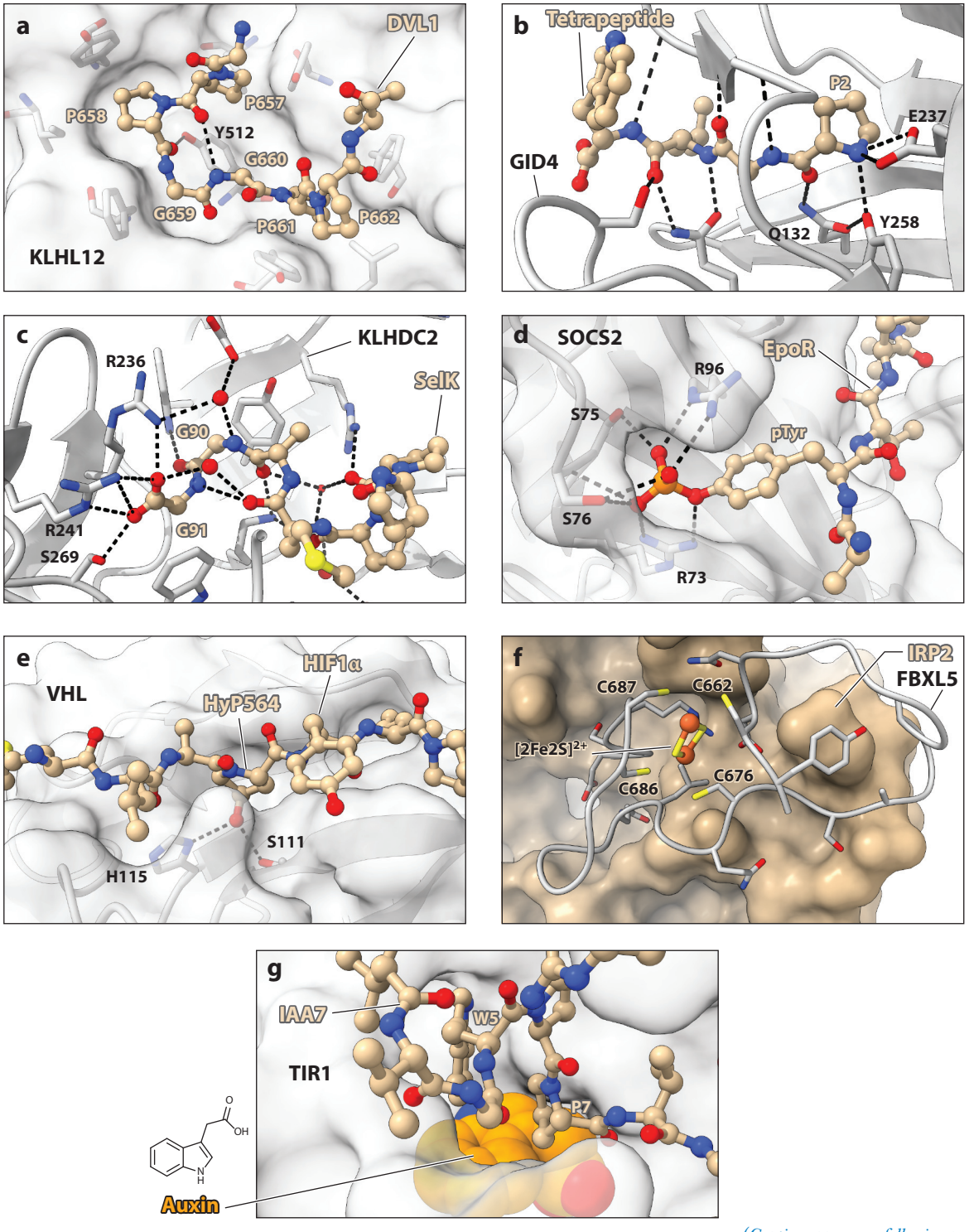

(*Caption appears on following page*)

Figure 3 (*Figure appears on preceding page*)

Recognition of substrates by E3 ligases in nature. Substrate receptors and substrates are colored gray and tan, respectively. Hydrogen bonds and ionic interactions are represented as black dotted lines. (*a*) X-ray crystal structure of substrate receptor KLHL12 in complex with substrate DVL1 peptide (PDB ID: 6TTK). The PGXPP motif residues of DVL1 are labeled, along with Tyr512, which forms a hydrogen bond with Pro658 of the peptide. Hydrophobic residues of KLHL12 lining the binding pocket are shown as sticks. (*b*) X-ray crystal structure of substrate receptor GID4 in complex with substrate Pro/N-degron PGLW tetrapeptide (PDB ID: 6CDC). Residues forming the hydrogen-bonding network between GID4 and the N-terminal proline residue of the tetrapeptide are labeled. (*c*) X-ray crystal structure of substrate receptor KLHDC2 in complex with the substrate SelK C-end degron peptide (PDB ID: 6DO3). Residues involved in the interactions with the carboxy terminus (Gly91) of the SelK peptide are labeled. (*d*) X-ray crystal structure of substrate receptor SOCS2 in complex with the substrate EpoR phosphodegron peptide (PDB ID: 6I4X). Hydrogen bonding and ionic interactions between residues of SOCS2 that interact with the phosphoryl group of the pTyr residue of the EpoR peptide are shown. (*e*) X-ray crystal structure of substrate receptor VHL in complex with the substrate HIF1α oxygen-dependent degron peptide (PDB ID: 1LM8). Hydrogen-bonding interactions between residues of VHL that interact with the hydroxyl group of HyP564 of HIF1α are shown. (*f*) Cryo-EM structure of substrate receptor FBXL5 (only the substrate-interacting interface loop and lid loop are shown for clarity) in complex with a $[2Fe2S]^{2+}$ cluster (*stick representation*) and the substrate IRP2 domain IV (PDB ID: 6VCD). $[2Fe2S]^{2+}$ cluster-coordinating cysteine residues are labeled, and residues of FBXL5 that interact with IRP2 are shown as sticks. (*g*) X-ray crystal structure of substrate receptor TIR1 in complex with small molecule hormone auxin (*sphere representation*, chemical structure depicted) and substrate IAA7 peptide (PDB ID: 2P1Q). Auxin binding creates a new molecular surface that interacts with Trp5 and Pro7 of the IAA7 peptide (*labeled*). Abbreviations: DVL, Dishevelled protein; EpoR, erythropoietin receptor; FBXL5, F-box and leucine rich repeat protein 5; GID4, glucose-induced degradation 4; HIF1α, hypoxia-inducible factor 1 alpha; HyP564, hydroxylated proline 564; IAA7, indoleacetic acid-induced protein 7; IRP2, iron regulatory protein 2; KLHDC2, Kelch domain–containing protein 2; KLHL12, Kelch-like protein 12; PDB ID, Protein Data Bank identifier; pTyr, phosphorylated tyrosine; SelK, selenoprotein K; SOCS, suppressor of cytokine signaling; TIR1, transport inhibitor response 1; VHL, von Hippel-Lindau tumor suppressor protein.

substrate receptor KLHL20 in complex with a peptide from its substrate DAPK1 (35), the CRL3 substrate receptor SPOP in complex with several substrate peptides (36, 37), and the cryo-EM structure of $CRL5^{ASB9}$ bound to its substrate creatine kinase brain-type (38).

The N and C termini of proteins can act as recognition motifs for N- and C-degron pathways, respectively (39, 40). N- and C-degrons may constitute either unmodified (type 1 substrate recognition) or modified (type 2 substrate recognition) N or C termini. Type 2 recognition may involve a cleavage event that exposes neo-N or neo-C termini degrons, and/or modification of terminal residues (e.g., N-terminal acetylation). Different N- and C-terminal residues and their modifications thereby dictate the half-lives of the protein in which they reside through the UPS. An example of a type 2 N-degron can be found in the yeast glucose-induced degradation (GID) protein complex that degrades gluconeogenic enzymes when glucose-starved yeast are transitioned to glucose-replete conditions (41, 42). The substrate-recognition subunit GID4 recognizes the N-terminal proline (N-Pro) residue of gluconeogenic enzymes that is exposed through cotranslational proteolytic removal of the initiator methionine by MetAPs (43, 44). The structure of the substrate receptor subunit GID4 was solved in complex with a tetrapeptide containing an N-Pro and showed a tight interaction network of hydrogen bonds between backbone atoms of the tetrapeptide and backbone and side chain atoms at the center of the GID4 β barrel (**Figure 3*b***) (45). The rigidity and increased basicity of proline in comparison to other amino acids explain why no other amino acids that are exposed by MetAP cleavage [Gly, Ala, Ser, Cys, Pro, Thr, and Val (44)] are tolerated in this position (43). An exquisite hydrogen- and ionic-bonding network centered around the proline residue, involving a hydrogen bond between the proline backbone carbonyl and the side chain of Gln132 of GID4, a hydrogen bond between the pyrrolidine nitrogen and the hydroxyl group of Tyr258 (which is in turn positioned by another hydrogen bond with Gln132), and a salt bridge between the pyrrolidine nitrogen and carboxyl group of Glu237 (**Figure 3*b***).

In addition to responses to environmental stimuli, some E3 ligases are involved in protein quality control. The Cul2 substrate receptor Kelch domain–containing protein 2 (KLHDC2)

recognizes and ubiquitinates polypeptides terminating in a C-terminal diglycine motif (46, 47). The motif is found in some full-length proteins but also in early-terminated fragments of selenoproteins SelK and SelS and the proteolytically generated N-terminal fragment of the deubiquitinating enzyme USP1. The crystal structure of KLHDC2 in complex with a SelK substrate peptide demonstrates an intricate hydrogen- and ionic-bonding network that is structurally licensed by the flexibility of the diglycine motif (**Figure 3*c***) (47).

Beyond proteolytic cleavage, type 2 substrate recognition occurs with many other PTM-generated degrons. The suppressor of cytokine signaling (SOCS) protein family inhibit cytokine signaling through the Janus kinase (JAK)/signal transducer and activator of transcription (STAT) pathway via several mechanisms, including acting as substrate receptors for Cul5–elonginB/C-type Cullin RING E3 ligases. They contain a SOCS box to recruit adaptor proteins elongin B and C and Cul5, as well as a Src-homology 2 (SH2) domain that binds to peptide motifs containing phosphorylated tyrosine residues in substrates. In addition, SOCS1 and SOCS3 possess a kinase inhibitory region, which inhibits the kinase activity of certain JAKs by blocking their substrate binding groove (48, 49). Structures of SOCS family SH2 domains, including those of SOCS1, SOCS2, SOCS3, and SOCS6, have been solved in complex with substrate or binding partner peptides (48–51). **Figure 3*d*** shows the SOCS2 SH2 domain in complex with a phosphorylated peptide from the erythropoietin receptor (EpoR), with the characteristic deep basic pocket lined by arginine and serine residues for phosphoryl-group binding (51).

In conditions of normal oxygen levels, the transcription factor HIF1α is *trans*-4-prolyl hydroxylated on proline residues 402 and 564 (52, 53). In another example of type 2 substrate recognition resulting from covalent PTM, the $CRL2^{VHL}$ E3 ligase binds the hydroxylated Pro564 (HyP564) residue, leading to constitutive ubiquitination and degradation. Under hypoxic conditions, HIF1α escapes proline hydroxylation, is therefore no longer degraded by $CRL2^{VHL}$, and can rapidly accumulate in the nucleus to activate expression of hypoxia response genes. The structure of the hydroxylated HIF1α peptide bound to VHL reveals how specificity for the hydroxylated form of HIF1α is achieved through a hydrogen-bonding network between Ser111 and His115 of VHL and the 4-hydroxyl group of the HyP564 side chain of HIF1α, as HyP564 adopts its preferred C4-exo ring pucker in order to fit snugly within the VHL binding pocket (**Figure 3*e***) (54, 55). While small molecule targeting of ubiquitous and charged interactions in phosphopeptide-binding proteins such as SOCS2 has proved difficult, the unique and relatively specific features of posttranslationally modified residues such as the hydroxylated HIF1α peptide inspired the structure-guided design of small molecule binders such as the VHL inhibitors VH032 and VH298 (56, 57). These VHL ligands are discussed further in the section titled Proteolysis-Targeting Chimeras.

Both type 2 and type 3 substrate recognition can also result from noncovalent modifications of protein structure through metabolite and small molecule binding. In another example of oxygen and also iron sensing, a combination of type 2 and type 3 substrate recognition occurs in the case of $CRL1^{FBXL5}$-mediated ubiquitination of iron regulatory protein 2 (IRP2) in iron- and oxygen-replete cells (58–64). Type 2 noncovalent allosteric recognition is dictated by iron–sulfur [4Fe4S] cluster insertion into IRP2, where cluster insertion induces a rotation of IRP domain III toward domain IV, sterically hindering the interaction with the substrate receptor F-box and leucine rich repeat protein 5 (FBXL5) (65). Type 3 noncovalent allosteric recognition includes both oxygen- and iron-dependent modification of the FBXL5 fold. Both the N-terminal hemerythrin-like domain and a C-terminal leucine-rich repeat (LRR) domain bind iron, as a diiron center and iron–sulfur [2Fe2S] cluster, respectively (65, 66). The conformation of the LRR domain is also coupled to cellular oxygen levels through the oxidation state of the iron–sulfur [2Fe2S] cluster (65). Four cysteine residues in the C-terminal loop region of FBXL5 fold around the oxidized form of the [2Fe2S] cluster, placing the interface loop in a conformation that can engage domain IV of the

substrate IRP2 (**Figure 3*f***), leading to its ubiquitination and degradation (65). Upon reduction of the $[2Fe2S]^{2+}$ cluster to $[2Fe2S]^{+}$ in conditions of hypoxia, FBXL5 binding to IRP2 is impaired, likely due to the interface loop adopting a conformation incompatible with IRP2 binding (65).

Certain plant hormone systems rely on type 3 noncovalent interfacial substrate recognition, with binding of the phytohormones auxin and jasmonate to their cognate CRL1 E3 ligase substrate receptors transport inhibitor response 1 (TIR1) and coronatine-insensitive 1 (COI1), respectively. In addition, type 3 noncovalent allosteric recognition occurs with binding of inositol polyphosphates (InsP) to both substrate receptors, influencing E3 ligase activity (67, 68). Hormone binding enables substrate recognition and ubiquitination; TIR1 recognizes and ubiquitinates the auxin/indoleacetic acid (AUX/IAA) repressor proteins, and COI1, the JAZ transcription factor. The structure of *Arabidopsis thaliana* TIR1 in complex with $InsP_6$, auxin, and a substrate peptide from AUX/IAA repressor indoleacetic acid-induced protein 7 (IAA7) revealed auxin bound to a pocket on TIR1, creating a new molecular surface to which IAA7 bound (**Figure 3*g***) (67). Auxin thereby acts as a molecular glue degrader, holding the two proteins together such that ubiquitination of the substrate is dependent on the presence of auxin (67). The next section of this review covers synthetic molecular glue degraders created in the laboratory and how they are able to bridge E3 ligases to neo-substrates that are not normally degraded in the absence of the chemical compound.

NEO-SUBSTRATE RECOGNITION IN TARGETED PROTEIN DEGRADATION

Molecular Glues

A small but growing number of synthetic molecular glue degraders induce de novo or stabilize weak protein–protein interactions (PPIs) to facilitate ubiquitination of neo-substrates in a manner reminiscent of the auxin and jasmonate plant hormone systems. Historically, these molecules have been discovered serendipitously through phenotypic screening campaigns, with their mode of action being elucidated later (69, 70). A schematic representation of the mechanism of action of a typical molecular glue is presented in **Figure 1*c***.

The first and most infamous example of synthetic molecules shown to function as molecular glue degraders are phthalimide-based immunomodulatory drugs (IMiDs). Thalidomide, the first-in-class phthalimide drug approved for use in the 1950s, caused severe birth defects when administered as a sedative to pregnant women. It was subsequently determined to be a potent teratogen (71). Though rapidly withdrawn from the market and banned for human use, thalidomide, and its analogs pomalidomide and lenalidomide, have since been found to be efficacious in treating select diseases, first leprosy and later some hematological cancers. The cellular target of IMiDs was identified as CRBN some six decades after thalidomide was first prescribed (72). Cocrystal structures of IMiDs bound to CRBN confirmed target engagement and revealed the binding site on the substrate-recognition subunit of the $CRL4^{CRBN}$ E3 ligase (73, 74). The mechanism of action was later determined to involve type 3 noncovalent interfacial substrate recognition, where phthalimide-bound CRBN recruits the neo-substrate zinc finger transcription factors Ikaros and Aiolos for ubiquitination and subsequent proteasomal degradation (75, 76). Other neo-substrates of IMiDs have since been identified with a common β-hairpin structural motif. The recent structure of the thalidomide metabolite 5-hydroxythalidomide (5HT) in complex with sal-like protein 4 (SALL4) (**Figure 4*a***) is especially notable, as degradation of SALL4 is thought to be responsible for the teratogenicity of the drug (77). As with the auxin structure, 5HT binds to a pocket on CRBN to create a new molecular surface that recruits the zinc finger 2 (ZF2) domain of SALL4 through its β-hairpin (77). Interestingly, when compared to thalidomide, the metabolite 5HT

displays altered neo-substrate specificity that can be rationalized by a structural comparison of the two drugs in complex with CRBN and SALL4 ZF2 (77). These findings suggest that small modifications to molecular glue degraders could tune specificity and may even lead to recruitment of additional neo-substrates. Many proteins are known or predicted to contain zinc fingers and a structurally conserved β-hairpin loop that could act as a potential structural degron and so classify as putative substrates of IMiD-bound CRBN (78).

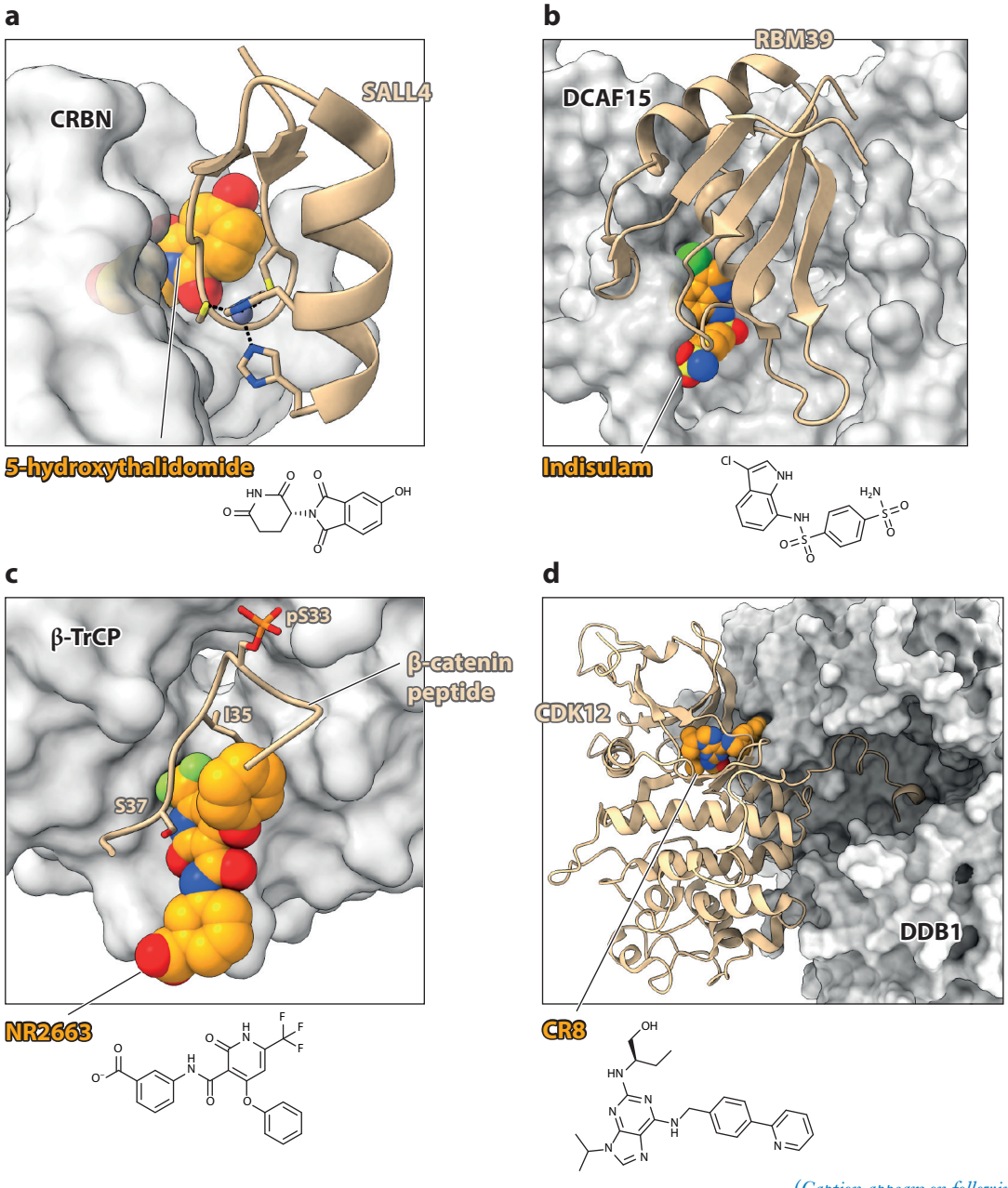

(*Caption appears on following page*)

Figure 4 (*Figure appears on preceding page*)

Ternary cocrystal structures of molecular glue degraders (*orange carbons*, chemical structure depicted) bound to E3 ligases (*gray*) and neo-substrates (*tan*). (*a*) X-ray crystal structure of substrate receptor CRBN in complex with molecular glue (*S*)-5-hydroxythalidomide and neo-substrate SALL4 (PDB ID: 7BQV). Zinc-coordinating residues of SALL4 are shown as sticks, and the zinc ion is shown as a sphere. (*b*) X-ray crystal structure of substrate receptor DCAF15 in complex with molecular glue indisulam and neo-substrate RBM39 (PDB ID: 6UD7). (*c*) X-ray crystal structure of substrate receptor β-TrCP in complex with molecular glue NR2663 and substrate β-catenin peptide (PDB ID: 6M92). Residues pSer33, Ile35, and Ser37 of the β-catenin peptide are shown as sticks and labeled. (*d*) X-ray crystal structure of adaptor protein DDB1 in complex with molecular glue CR8 and neo-substrate receptor CDK12 (PDB ID: 6TD3). Abbreviations: β-TrCP, beta-transducin repeat containing protein; CDK, cyclin-dependent kinase; CRBN, cereblon; DCAF15, DDB1- and CUL4-associated factor 15; DDB1, DNA damage–binding protein 1; PDB ID, Protein Data Bank identifier; RBM39, RNA-binding motif protein 39; SALL4, sal-like protein 4.

The anticancer aryl-sulfonamide compounds, including indisulam and E7820, exert their antiproliferative effects by acting as molecular glues. The compounds recruit RNA-binding motif proteins (RBMs), specifically RBM39 and to a lesser extent RBM23, to the CRL4 substrate receptor DNA damage–binding protein 1 (DDB1)- and CUL4-associated factor (DCAF) 15, with the antiproliferative effect mediated through RBM39 ubiquitination and degradation (79, 80). Three papers revealed the structural determinants of aryl-sulfonamide compound binding and gluing (81–83), and the structure of indisulam in complex with DCAF15 and RBM39 is presented in **Figure 4*b*** (the CRL4 adaptor protein DDB1 and accessory protein DET1- and DDB1-associated protein 1 were also part of the complex but are not depicted). Although the complexes formed between aryl-sulfonamide compounds, DCAF15, and RBM39 are stable and long-lived, the compounds alone have micromolar (E7820) to undetectable (indisulam and tasisulam) affinity for DCAF15 and undetectable affinity for RBM39 in binary interactions (81–83). This phenomenon likely arises from the large protein–protein interface between DCAF15 and RBM39 on top of the more minor but essential interactions the glues contribute. **Table 1** shows the buried surface area contributions of each component to the overall assembly for this structure and for other molecular glue and PROTAC ternary structures covered in this review. An interesting comparison can be made to the CRBN–5HT–SALL4 complex, where the binary K_D between the *S* enantiomer of 5HT and CRBN is $0.76 \pm 0.20\,\mu M$. The CRBN–SALL4 interface has an interface area of 479.1 Å^2 with a Δ^iG of −0.2 kcal/mol, Δ^iG P value of 0.670, 7 hydrogen bonds, and no salt bridges, as calculated using PISA (84, 85). See the PDBePISA webserver for definitions of the Δ^iG and Δ^iG P values, and note that all further interface analyses in this review were performed with PISA. These values are similar to those seen in crystal contacts, whereas the interface between DCAF15 and RBM39 is more extensive and reminiscent of a native protein–protein interface. The DCAF15–RBM39 interface encompasses an area of 1209.8 Å^2, and the surface area has many hydrophobic interactions, which contribute to a Δ^iG of −8.0 kcal/mol, Δ^iG P value of 0.501, 11 hydrogen bonds, and 7 salt bridges (see **Supplemental Table 1** for detailed PISA-generated statistics of interfaces and assemblies in the ternary structures induced by molecular glues and PROTACs). In comparison to the CRBN system, the extensiveness of the sulfonamide-induced DCAF15-RBM39 interface may compensate for the weak affinity between glue and E3 ligase in formation of a stable ternary complex.

Supplemental Material >

Though the majority of currently known molecular glue degraders discovered through phenotypic screens have been identified retrospectively, targeted screens to find glues that enhance E3 ligase–substrate interactions have also yielded interesting compounds. Type 2 interfacial substrate recognition of the doubly phosphorylated phosphodegron of the oncogenic transcription factor β-catenin by its cognate E3 $CRL1^{\beta\text{-}TrCP}$ leads to its ubiquitination and degradation (86, 87). Mutations to β-catenin or decreased levels of phosphorylation can weaken

Table 1 Buried surface area of molecular glue and PROTAC ternary complexes. Buried surface area of the interfaces involved in the ternary complex were calculated with PISA (84)

Degrader type	Ligand	Ligase	Target	Method	PDB ID	Resolution	Buried surface area in ternary complex interface (Å^2)				Percentage total buried surface area of complex (%)		
							Ligase-target	Ligase-ligand	Target-ligand	Total interface	Ligase-target	Ligase-ligand	Target-ligand
Molecular Glue	2,4-D	$SKP1^{TIR1}$	IAA7 peptide	X-ray	2P1N	2.50 Å	664	223	68	954	70	23	7
	1-NAA	$SKP1^{TIR1}$	IAA7 peptide	X-ray	2P1O	1.90 Å	720	214	70	1003	72	21	7
	Auxin	$SKP1^{TIR1}$	IAA7 peptide	X-ray	2P1Q	1.91 Å	656	202	68	926	71	22	7
	Lenalidomide	$CRL4^{CRBN}$	CK1α	X-ray	5FQD	2.45 Å	582	234	99	916	64	26	11
	CC-885	$CRL4^{CRBN}$	GSPT1	X-ray	5HXB	3.60 Å	601	331	232	1164	52	28	20
	Pomalidomide	$CRL4^{CRBN}$	IKZF1 (ZF2)	X-ray	6H0F	3.25 Å	521	237	101	858	61	28	12
	Pomalidomide	$CRL4^{CRBN}$	ZNF692 (ZF4)	X-ray	6H0G	4.25 Å	540	249	91	880	61	28	10
	NRX-2776	$SKP1^{β\text{-}TrCP}$	β-catenin peptide	X-ray	6M90	2.05 Å	480	247	151	877	55	28	17
	NRX-103094	$SKP1^{β\text{-}TrCP}$	β-catenin peptide	X-ray	6M91	2.40 Å	563	242	200	1005	56	24	20
	NRX-2663	$SKP1^{β\text{-}TrCP}$	β-catenin peptide	X-ray	6M92	2.35 Å	534	247	170	950	56	26	18
	NRX-1933	$SKP1^{β\text{-}TrCP}$	β-catenin peptide	X-ray	6M93	2.50 Å	502	195	112	809	62	24	14
	E7820	$CRL4^{DCAF15}$	RBM39	X-ray	6PAI	2.90 Å	933	320	132	1386	67	23	10
	Indisulam	$CRL4^{DCAF15}$	RBM39	Cryo-EM	6SJ7	3.54 Å	1161	298	169	1628	71	18	10
	CR8	$CRL4^{\Delta}$	cyclin K	X-ray	6TD3	3.46 Å	2105	147	420	2672	79	5	16
	Indisulam	$CRL4^{DCAF15}$	RBM39	X-ray	6UD7	2.30 Å	1210	298	162	1670	72	18	10
	Pomalidomide	$CRL4^{CRBN}$	SALL4 (ZF2)	X-ray	6UML	3.58 Å	352	239	90	681	52	35	13
	CC-90009	$CRL4^{CRBN}$	GSPT1	X-ray	6XK9	3.64 Å	658	330	233	1221	54	27	19
	Thalidomide	$CRL4^{CRBN}$	SALL4 (ZF2)	X-ray	7BQU	1.90 Å	394	223	89	706	56	32	13
	5HT	$CRL4^{CRBN}$	SALL4 (ZF2)	X-ray	7BQV	1.80 Å	479	230	93	802	60	29	12

(*Continued*)

Table 1 (*Continued*)

Degrader type	Ligand	Ligase	Target	Method	PDB ID	Resolution	Buried surface area in ternary complex interface (Å^2)				Percentage total buried surface area of complex (%)		
							Ligase-target	Ligase-ligand	Target-ligand	Total interface	Ligase-target	Ligase-ligand	Target-ligand
PROTAC	MZ1	$CRL2^{VHL}$	BRD4 (BD2)	X-ray	5T35	2.70 Å	343	506	489	1338	26	38	37
	dBET23	$CRL4^{CRBN}$	BRD4 (BD1)	X-ray	6BN7	3.50 Å	519	306	503	1328	39	23	38
	dBET6	$CRL4^{CRBN}$	BRD4 (BD1)	X-ray	6BOY	3.33 Å	550	321	424	1294	42	25	33
	PROTAC 2	$CRL2^{VHL}$	SMARCA2	X-ray	6HAX	2.35 Å	320	456	348	1125	28	41	31
	PROTAC 1	$CRL2^{VHL}$	SMARCA2	X-ray	6HAY	2.24 Å	329	476	365	1171	28	41	31
	PROTAC 2	$CRL2^{VHL}$	SMARCA4	X-ray	6HR2	1.76 Å	324	461	350	1135	29	41	31
	MacroPROTAC-1	$CRL2^{VHL}$	BRD4 (BD2)	X-ray	6SIS	3.50 Å	326	484	551	1361	24	36	40
	Compound 9	$CRL4^{DCAF15}$	RBM39	X-ray	6UE5	2.61 Å	1197	305	156	1658	72	18	9
	BCPyr	$cIAP^{BIR3}$	BTK	X-ray	6W7O[a]	2.17 Å	513	390	532	1435	36	27	37
	BC5P	$cIAP^{BIR3}$	BTK	X-ray	6W8I	3.80 Å	367	387	636	1389	26	28	46
	PROTAC6	$CRL2^{VHL}$	BCL-X_L	X-ray	6ZHC	1.92 Å	308	458	778	1543	20	30	50
	Compound 9	$CRL2^{VHL}$	BRD4 (BD1)	X-ray	7KHH	2.28 Å	353	384	499	1236	29	31	40

Abbreviations: 5HT, 5-hydroxythalidomide; β-TrCP, beta-transducin repeat containing protein; BCL-X_L, B-cell lymphoma-extra large; BD, bromodomain; BIR3, baculoviral-IAP repeat domain 3; BRD4, bromodomain and extraterminal domain protein; BTK, Bruton's tyrosine kinase; cIAP, cellular inhibitor of apoptosis 1; CK1α, casein kinase I isoform alpha; CRBN, cereblon; CRL, Cullin–RING ligase; cryo-EM, cryo–electron microscopy; DCAF15, DNA damage–binding protein 1– and cullin 4-associated factor 15; GSPT1, eukaryotic peptide chain release factor GTP-binding subunit ERF3A; IAA7, indoleacetic acid-induced protein 7; IKZF1, IKAROS family zinc finger 1; PDB ID, Protein Data Bank identifier; PROTAC, proteolysis-targeting chimera; RBM39, RNA-binding motif protein 39; SALL4, sal-like protein 4; SKP1, S-phase kinase-associated protein 1; SMARCA, SWI/SNF related, matrix associated, actin dependent regulator of chromatin, subfamily A; TIR1, transport inhibitor response 1; VHL, von Hippel-Lindau tumor suppressor protein; ZF2/4, zinc finger 2/4 domain; ZNF692, zinc finger protein 692.
[a]The highest surface area interaction of the three unique potential complexes was chosen.

the interaction with CRL1$^{\beta\text{-TrCP}}$, stabilizing β-catenin and leading to constitutive Wnt signaling in most colorectal cancers (88, 89). A targeted screen to stabilize the interaction between monophosphorylated mutant β-catenin and CRL1$^{\beta\text{-TrCP}}$ identified a hit that was improved by structure-guided design. This study resulted in small molecule glue compounds that enhanced affinity for a monophosphorylated pSer33 β-catenin peptide by >10,000-fold (90). The crystal structure of S-phase kinase-associated protein 1 (Skp1)–β-TrCP in complex with the monophosphorylated pSer33 β-catenin peptide and the glue NRX-2663 shows the compound filling the binding pocket normally occupied by the second phosphoryl group at Ser37 of the doubly phosphorylated peptide, holding the β-catenin peptide and substrate receptor β-TrCP together (**Figure 4*c***) (90).

The discovery of molecular glue degraders has generally been driven through phenotypic screening for efficacious compounds rather than directly searching for compounds with degrader activity. A recent study set out to identify compounds with glue degrader properties by correlating drug-sensitivity data for clinical and preclinical drugs tested in cancer cell lines with mRNA levels of 499 E3 ligase components (91). The CRL4 substrate receptor DCAF15 was used as a proof of principle, with the sensitivity of known aryl-sulfonamide degraders indisulam and tasisulam correlating with mRNA levels of DCAF15 across the drug-sensitivity data set. The cyclin-dependent kinase (CDK) inhibitor CR8 emerged as a potential degrader through correlation of CR8 sensitivity with mRNA levels of the CRL4 adaptor DDB1. These examples of glue degraders involve the complexation of substrates and neo-substrates directly with the substrate receptors of CRLs. Somewhat surprisingly, mRNA levels for known CRL4 substrate receptors that bind DDB1 did not correlate with sensitivity to CR8. Quantitative proteome-wide mass spectrometry revealed cyclin K was depleted in CR8-treated cells as opposed to any CDK to which CR8 binds. Instead of recruiting a neo-substrate to an E3 substrate receptor, CR8 functions through an unprecedented mechanism, whereby a CR8-bound CDK12–cyclin K complex is glued directly to the DDB1 adaptor protein. Two other groups identified and validated other compounds that glue CDK12 to DDB1 at approximately the same time through different methods, suggesting that many compounds that engage the ATP-binding pocket of CDK12 can function as molecular glues for the DDB1–CDK12 interaction (92, 93). The crystal structure of DDB1 in complex with CR8, CDK12, and cyclin K shows CR8 bound to the ATP-binding pocket of CDK12 and the β-propeller C (BPC) domain of DDB1 (**Figure 4*d***) (91). The PPIs between DDB1 and CDK12 are extensive. The C-lobe of CDK12 interacts with the β-propeller A (BPA) domain of DDB1, while the C-terminal tail of CDK12 binds to the cleft between the BPA and BPC domains. This latter site is responsible for binding cognate CRL4 substrate receptors such as CRBN and DCAF family proteins. Cyclin K is engaged with CDK12 distal to the interactions with DDB1 and makes no direct contact with the adaptor protein. Thus, CDK12 acts as a neo-substrate receptor that recruits its cognate binding partner, cyclin K, for ubiquitination by CRL4.

A novel avenue to TPD has recently been highlighted in the case of the oncogenic nonenzymatic transcription factor B-cell lymphoma 6 (BCL6). The BCL6 inhibitor BI-3802 induces polymerization of BCL6 into filamentous structures, acting as a molecular glue between BCL6 homodimers (94). This small-molecule-mediated polymerization of BCL6 accelerates its ubiquitination by the non-Cullin E3 ligase seven *in absentia* homolog 1 (SIAH1) that recognizes a VxP degron motif. The affinity of the SIAH1 for BCL6 is greatly enhanced in the presence of BI-3802, likely due to cooperativity from the polymerization of BCL6. This mechanism of action, which may be widely applicable to symmetrical proteins where there is potential to induce polymerization, has great therapeutic potential due to its specificity: Only the target is polymerized then degraded by its cognate E3 ligase.

Proteolysis-Targeting Chimeras

Since the 2015 studies disclosing significantly improved PROTACs based on VHL and CRBN ligands, as mentioned in the introduction, the field has witnessed an exponential growth in papers, patents, and undisclosed drug discovery programs featuring PROTAC molecules. The expanding diversity of PROTAC chemistries, biological targets, and therapeutic avenues are extensively reviewed elsewhere (95–98). Here, we focus on structural studies that have contributed to illuminating PROTAC mechanisms of molecular recognition.

Unlike molecular glues, which are generally monovalent and bind primarily to either the neo-substrate or the E3 ligase, PROTACs are multivalent molecules that contain individual binding moieties covalently attached through a chemical linker. Each binding group can engage independently with the target neo-substrate or the E3 to be recruited; the formation of a ternary 1:1:1 complex consisting of the neo-substrate, the PROTAC, and the E3 is what elicits degradation. As such, PROTACs were initially thought to work independently of PPIs and primarily by a tethering mechanism that induced proximity. In this model, ubiquitination occurs when the PROTAC tethers the neo-substrate to the E3 in close but highly flexible proximity. Structural and biophysical data have since shown that PROTACs can also function similarly to molecular glues in that they can induce neo-PPIs between the E3 and the target protein that contribute to the formation of stable and cooperative ternary complexes between neo-substrate, PROTAC, and E3 (99). Cooperativity (α) is defined as the ratio of the dissociation constants for a given PROTAC binding to one binding partner (e.g., the neo-substrate) in the absence (binary K_D) and presence (ternary K_D) of the second binding partner (e.g., the E3 ligase) ($\alpha = K_D^{\text{binary}}/K_D^{\text{ternary}}$) (99). Cooperativity can be positive (wherein PPIs enhance ternary complex formation), noncooperative (wherein PPIs neither enhance nor inhibit ternary complex formation), or negative (wherein steric clashes and other factors inhibit ternary complex formation). The stability and positive cooperativity of ternary complexes correlate with more efficient degradation of neo-substrates where the ternary complex is productive, i.e., substrate positioning is such that a lysine residue on its surface can undergo E2-catalyzed ubiquitination (100, 101).

The first structural insight into PROTAC ternary complex formation came from the PROTAC *MZ1*, a $CRL2^{VHL}$-recruiting degrader of the transcriptional regulator bromodomain and extraterminal domain (BET) proteins bromodomain-containing protein (BRD)2, BRD3, and BRD4 (99). BET family proteins regulate cell proliferation and cell cycle progression and have become targets of therapeutic interest in cancer, neurological disorders, and inflammation (102, 103). The crystal structure of the substrate receptor VHL (complexed with the adaptor proteins elongin B and C here and in other structural examples in this section) bound to *MZ1* and the second bromodomain (BD2) of BRD4 revealed *MZ1* engaged in the expected binary binding interactions with VHL through its VH032 moiety and BRD4's BD2 through its JQ1 moiety (**Figure 5*a***) (99). In addition to these protein–ligand interactions, the flexible polyethylene glycol linker collapses and interacts favorably with BRD4. VHL and BRD4 shield parts of JQ1 and VH032, respectively, that would otherwise be solvent exposed in the binary complexes. Due to the extensive, isoform-specific PROTAC-induced PPIs between VHL and BRD4, ternary complex formation is highly cooperative ($\alpha = 18$) and long-lived ($t_{1/2} > 2$ min), explaining the preferential degradation of BRD4 by *MZ1* over the other BET proteins BRD2 and BRD3, despite the parent compound JQ1 being a pan-specific BET inhibitor (100). The structure of the ternary complex informed the design of an even more selective BRD4 degrader, AT1, as well as a macrocyclic PROTAC, macroPROTAC-1, which constrains the PROTAC in its bioactive conformation (**Figure 5*b***) (99, 104). The macrocyclization design strategy was shown to be effective, as macroPROTAC-1 degradation activity was comparable to that of its parent noncyclic *MZ1*, despite losing more than tenfold binding affinity for the BET bromodomain due to steric clashes from the added cyclizing linker (104).

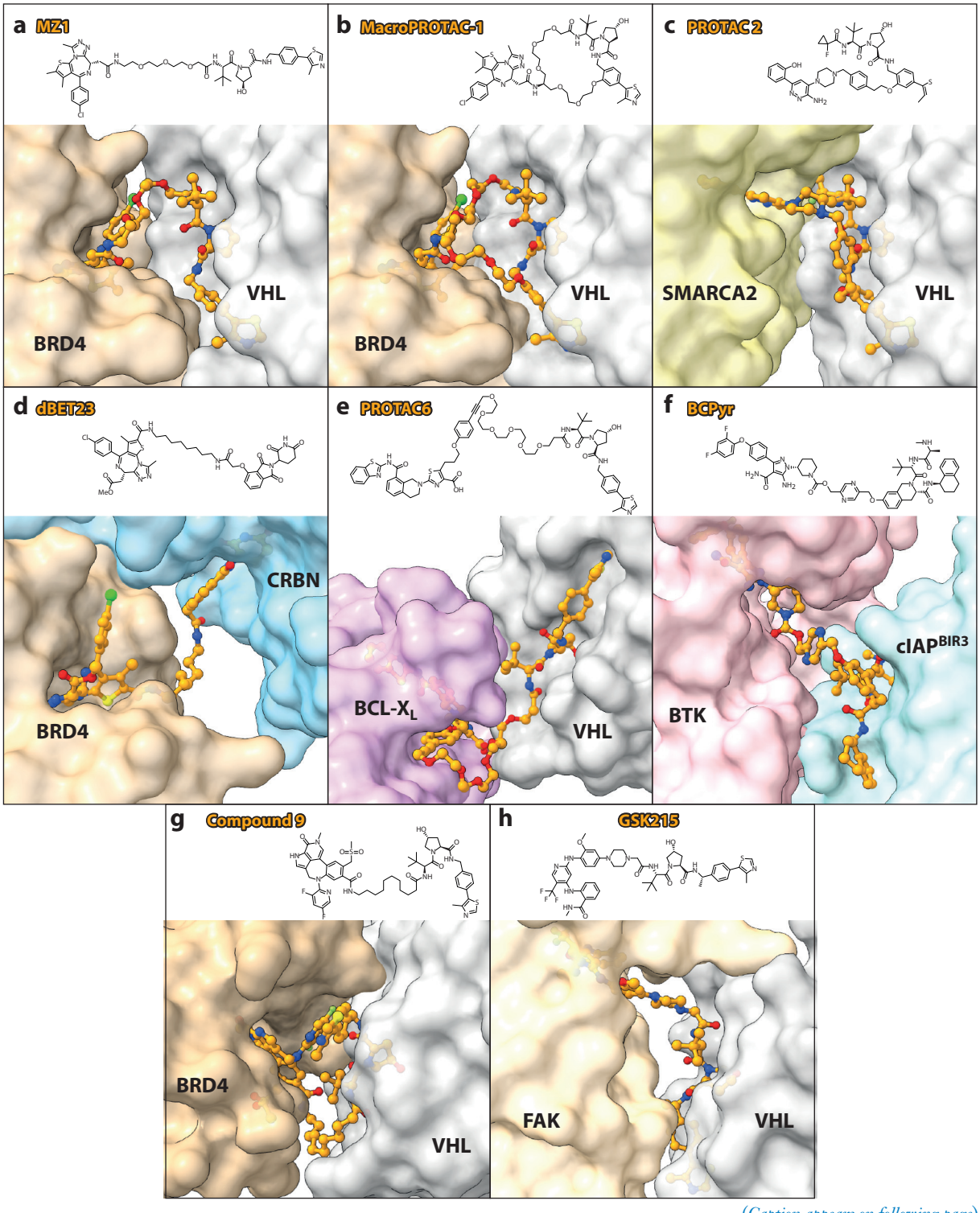

(*Caption appears on following page*)

Figure 5 (*Figure appears on preceding page*)

Ternary complex cocrystal structures of heterobifunctional PROTAC degraders (*orange carbons*, chemical structure depicted) bound to E3 ligases and neo-substrate targets. (*a*) X-ray crystal structure of the ternary complex of neo-substrate BRD4, the PROTAC MZ1, and substrate receptor VHL (PDB ID: 5T35). (*b*) X-ray crystal structure of the ternary complex of neo-substrate BRD4, macroPROTAC-1, and substrate receptor VHL (PDB ID: 6SIS). (*c*) X-ray crystal structure of the ternary complex of neo-substrate SMARCA2, PROTAC 2, and substrate receptor VHL (PDB ID: 6HAX). (*d*) X-ray crystal structure of the ternary complex of neo-substrate BRD4, the PROTAC dBET23, and substrate receptor CRBN (PDB ID: 6BN7). (*e*) X-ray crystal structure of the ternary complex of neo-substrate BCL-X_L, PROTAC6, and substrate receptor VHL (PDB ID: 6ZHC). (*f*) X-ray crystal structure of the ternary complex of neo-substrate BTK, the PROTAC BCPyr, and substrate receptor $cIAP^{BIR3}$ (PDB ID: 6W7O). (*g*) X-ray crystal structure of the ternary complex of neo-substrate BRD4, the PROTAC Compound 9, and substrate receptor VHL (PDB ID: 7KHH). (*h*) X-ray crystal structure of the ternary complex of neo-substrate FAK, the PROTAC GSK215, and substrate receptor VHL (PDB ID: 7PI4). Abbreviations: BCL-X_L, B-cell lymphoma-extra large; BIR3, baculoviral-IAP repeat domain 3; BRD, bromodomain and extraterminal domain protein; BTK, Bruton's tyrosine kinase; cIAP, cellular inhibitor of apoptosis; CRBN, cereblon; FAK, focal adhesion kinase; PDB ID, Protein Data Bank identifier; PROTAC, proteolysis-targeting chimera; SMARCA, SWI/SNF related, matrix associated, actin dependent regulator of chromatin, subfamily A; VHL, von Hippel-Lindau tumor suppressor protein.

Structure-based design has also generated potent $CRL2^{VHL}$-recruiting degraders of another bromodomain-containing protein family: the SWI/SNF related, matrix associated, actin dependent regulator of chromatin, subfamily A (SMARCA) proteins SMARCA2 and SMARCA4 (105). After an initial round of PROTAC design and screening using a SMARCA bromodomain ligand (106, 107) and the potent VHL binder VH101 (108), PROTAC 1 was identified as a partial degrader of SMARCA2 and SMARCA4. This compound exhibited positive cooperativity ($\alpha = 4.8$) for ternary complex formation, as measured by isothermal titration calorimetry. The crystal structure of the ternary complex revealed the expected binary interactions between the respective protein-binding moieties of the PROTAC and their targets, as well as PROTAC-induced PPIs between VHL and the SMARCA2 bromodomain. Structure-guided optimization of the linker to rigidify it, pick up a π-stacking interaction with VHL Y98, and increase lipophilicity led to PROTAC 2, which exhibited more favorable ternary complex formation and cellular permeability. Another pair of crystal structures of ternary complexes induced by PROTAC 2 with both the SMARCA2 (**Figure 5*c***) and SMARCA4 bromodomains revealed the linker π-stack with VHL Y98 had been picked up as designed, with minimal changes to the rest of the binding mode. Further linker optimization led to ACBI1, a PROTAC with an α value of ∼30 and a half-maximal target degradation of 6 and 11 nM for SMARCA2 and SMARCA4, respectively, an almost 50-fold improvement for SMARCA2 and 22-fold for SMARCA4 over the original PROTAC 1 (105).

These studies support the formation of stable and cooperative ternary complexes as key intermediate species driving favorable and efficient protein ubiquitination. Nonetheless, positive cooperativity is not strictly required for efficient degradation of target proteins by PROTACs, as was shown both for VHL-based PROTACs that degrade BET proteins (109) and for IMiD-based $CRL4^{CRBN}$-recruiting dBET PROTACs that degrade BRD4 (110). VHL-based MZP-type PROTAC degraders all exhibited negative cooperativity and were poorer degraders than the MZ-type PROTACs, despite being designed from BET inhibitors that had more than tenfold greater binding affinity for the BET bromodomains (109). Still, they were able to act as degraders, albeit with a narrower pharmacological range and earlier onset of the hook effect [where at higher concentrations, the target and E3 binding sites become saturated, leading to nonproductive binary complexes (111)] compared to the MZ1 PROTAC. The CRBN-based dBET degraders exhibited varying levels of negative cooperativity with the individual BRD4 bromodomains BD1 and BD2; however, their cooperativity values were still generally proportional to their cellular dBET activity. Despite negative cooperativity being indicative of unfavourability for ternary complex formation, the structures of CRBN and BRD4 BD1 complexes with several dBETs were determined (110). Due to poor resolution (3.3 Å or lower), the dBET used was modelled only in two of the

Supplemental Material >

five structures reported. Comparisons of the interface and assembly properties of these and other low-resolution structures with the higher resolution structures in **Table 1** and **Supplemental Table 1** should be made with caution. The ternary structure of CRBN, dBET23, and BRD4 BD1 is presented in **Figure 5*d***. Taken together, the structures reveal BRD4 BD1 binds different surfaces of CRBN depending on the dBET used, recapitulating the mutagenesis data from the same study. Docking of lenalidomide-bound CRBN and JQ1-bound BRD4 BD1 was performed in the absence of degraders to look for low energy minima, and potential docking poses with the shortest distance between the lenalidomide and JQ1 were used for degrader design. The resulting optimized compound using a different linker point on JQ1, ZXH-3-26, showed more selective degradation of BRD4 BD1 over other truncated BRD2, BRD3, and BRD4 bromodomains, compared to dBET6, MZ1, and dBET57, each of which degraded at least one other bromodomain.

Another structure of a ternary complex with a negatively cooperative PROTAC has recently been solved, that of a $CRL2^{VHL}$-recruiting B-cell lymphoma-extra large ($BCL\text{-}X_L$) PROTAC degrader, PROTAC 6 (**Figure 5*e***) (112). $BCL\text{-}X_L$ is an antiapoptotic BCL-2 family protein of therapeutic interest for the treatment of many cancers (113, 114), but the use of $BCL\text{-}X_L$ inhibitors is complicated by on-target dose-limiting thrombocytopenia because platelets depend on $BCL\text{-}X_L$ for survival (115). Platelets express low levels of VHL, and $CRL2^{VHL}$-recruiting PROTACs targeting $BCL\text{-}X_L$ circumvent the toxicity issues associated with $BCL\text{-}X_L$ inhibition, leaving platelet populations largely intact (116). PROTAC 6 was developed using a highly selective and potent $BCL\text{-}X_L$ inhibitor (117). Interestingly, despite the slight negative cooperativity, PROTAC 6 induces several neo-PPIs between $BCL\text{-}X_L$ and VHL, including a salt bridge between Asp133 of $BCL\text{-}X_L$ and Arg60 of VHL. As in the comparison of indisulam and 5HT outlined in the section titled Molecular Glues, comparisons of the properties of the protein–protein interfaces between the substrate receptor and neo-substrate induced by the positively cooperative MZ1 versus the negatively cooperative PROTAC 6 provide interesting insights. Between the two copies of the complex in the asymmetric unit (ASU) of the MZ1 PROTAC structure, the BRD4–VHL interface has an average Δ^iG value of −1.5 kcal/mol and average Δ^iG P value 0.59 and also includes up to 7 hydrogen bonds and 7 salt bridges, values suggestive of a weak native PPI (84, 85). However, the protein–protein interface induced by PROTAC 6 between $BCL\text{-}X_L$ and VHL has a positive Δ^iG value of 2.9 kcal/mol, a Δ^iG P value of 0.849, no hydrogen bonds, and 1 salt bridge, values more suggestive of a crystal contact–like interface (84, 85).

Two ternary crystal structures of a noncooperative and an optimized positively cooperative cellular inhibitor of apoptosis 1 (cIAP1)-recruiting PROTAC degrader of Bruton's tyrosine kinase (BTK) have recently been reported. The initial structure of the noncooperative degrader BC5P in complex with cIAP1 baculoviral-IAP repeat domain 3 (BIR3) and BTK revealed 3 PROTAC-induced ternary complexes in the ASU, all with different orientations of BTK in relation to $cIAP^{BIR3}$ and different PPIs. As with the dBET structures, the low resolution of this structure precludes accurate analysis of the PPIs. However, manual examination of the structure reveals minimal contacts between the substrate receptor and neo-substrate for two of the copies of the ternary complex in the ASU and a slightly larger interface for the third copy. The structure of the linker-optimized, positively cooperative degrader BCPyr in complex with $cIAP1^{BIR3}$ and BTK reveals two copies of the $cIAP^{BIR3}$–BCPyr–BTK complex in the ASU (**Figure 5*f***). The protein–protein interfaces between $cIAP1^{BIR3}$ and BTK have an average Δ^iG value of −1.55 kcal/mol, average Δ^iG P value of 0.603, and the presence of up to 8 hydrogen bonds and 3 salt bridges, values similar to those observed for the VHL–MZ1–BRD4 complex (84, 85). Despite the increase in cooperativity when moving from BC5P to BCPyr, BC5P was a superior degrader of BTK in cellular assays. While many factors can affect the cellular potency of PROTACs, including the compounds' cell permeability, the similarity of the calculated properties of BC5P and BCPyr suggests

the difference in potency may be due to the greater degree of flexibility in the cIAP^{BIR3}–BC5P–BTK complexes. This flexibility may allow better access of the E3 ligase to BTK lysine residues as compared to the more rigid cIAP^{BIR3}–BCPyr–BTK complex. This study and the work with dBET degraders suggest stable and rigid ternary complexes may not always lead to the most efficient degradation of target proteins, possibly due to the requirement for a degron to have a lysine residue on the target protein that is accessible to the recruited E3 ligase for ubiquitin attachment.

Positive cooperativity helps to augment the stability of PROTAC ternary complexes, thereby enhancing the chances of cocrystallizing the complex. Two final examples of positively cooperative PROTAC ternary complex structures have been reported recently. The first structure was determined as part of a large campaign using antibody–drug conjugates incorporating CRL2^{VHL}-recruiting, BRD4-targeting degraders that deliver the PROTACs to cells (118, 119). The structure, consisting of VHL, compound 9, and BRD4, is presented in **Figure 5*g*** (119). Although the authors do not report a cooperativity value for their PROTAC (compound 9), the long half-life of the ternary complex as measured by surface plasmon resonance is suggestive of positive cooperativity. With this in mind, it is not surprising that the protein–protein interface induced by compound 9 is more reminiscent of a weak native protein–protein interface similar to the VHL–MZ1–BRD4 complex, with a $\Delta^{i}G$ value of −3.6 kcal/mol, 3 hydrogen bonds, and 3 salt bridges (84, 85). Still, the PROTAC induces the formation of a unique ternary complex where the orientation of the BRD4 bromodomain and VHL differs dramatically from that of the VHL–MZ1–BRD4 complex. These findings suggest that, at least in the context of BRD4–VHL, very different orientations of neo-substrate relative to E3 ligase can still result in substrate ubiquitination.

The last structure we cover is that of a CRL2^{VHL}-recruiting PROTAC degrader of focal adhesion kinase (FAK, also known as PTK2) (120), an important cancer target in solid tumors that is associated with poor clinical outcomes (121, 122). FAK-degrading PROTACs active in cellular assays had previously been reported by groups at Yale University (CRL2^{VHL}-recruiting), Boehringer Ingelheim/the University of Dundee (CRL2^{VHL}- or CRL4^{CRBN}-recruiting), and Tsinghua University (CRL4^{CRBN}-recruiting) (123–125). Although some have since been shown to be active in mouse models (126–128), biophysical characterization of ternary complex formation and structure were lacking prior to work by Law et al. (120). In this study, PROTACs were designed based on the FAK inhibitor VS-4718/PND-1186 (129) and the VHL ligand (130) with different linkers. Using Förster resonance energy transfer assays to measure cooperativity, positive cooperativity was observed for all compounds. Higher cooperativity was correlated with greater potency of degradation. GSK215, which has an unusually short acetamide linker, displayed the most potent degradation of FAK in cellular assays and an extremely high cooperativity α factor of 104, and was crystallized in complex with VHL and FAK. The ternary structure reveals several neo-PPIs between VHL and FAK (**Figure 5*b***), including both hydrogen bonds and salt bridges. Interestingly, a large interaction surface area in the ternary complex is contributed by the sandwiching of the VHL ligand between VHL and the αD helix in the C-lobe of FAK. The phenyl ring of the VHL ligand sits in a hydrophobic pocket formed by the peptide backbone between Gln512 and Val513 of the αD helix.

CONCLUDING REMARKS

The biochemical and structural investigations of E3 ligases continue to bear fruit and reveal expanding modes of recognition. They provide insight into how substrates and neo-substrates can be recruited, ubiquitinated, and then degraded. They also reveal how small molecules can bridge the substrate and ligase to induce interactions through ternary complexes of diverse orientations and geometries and with distinct thermodynamic and kinetic features. The original molecular glue

degraders that have been discovered and characterized so far are monovalent and therefore strictly require a high level of cooperativity to stabilize complexes favorably for productive ubiquitination. The discovery and structural understanding that bivalent PROTACs also exhibit a high propensity to glue neo-substrates to E3 ligases have revealed how molecular recognition can be exploited to drive productive ubiquitination and rapid and efficient target degradation. The mechanism of enhancing proximity and inducing PPIs between proteins is emerging as much more prevalent than previously anticipated. This realization may have important functional and mechanistic implications that can be exploited to target other enzymatic and nonenzymatic systems beyond E3 ligases.

DISCLOSURE STATEMENT

The Ciulli laboratory receives or has received sponsored research support from Almirall, Amgen, Amphista Therapeutics, Boehringer Ingelheim, Eisai, Merck KGaA, Nurix Therapeutics, and Ono Pharmaceutical. A.C. is a scientific founder, shareholder, and advisor of Amphista Therapeutics, a company that is developing targeted protein degradation therapeutic platforms.

ACKNOWLEDGMENTS

Molecular graphics and analyses performed with UCSF ChimeraX, developed by the Resource for Biocomputing, Visualization, and Informatics at the University of California, San Francisco, with support from National Institutes of Health R01-GM129325 and the Office of Cyber Infrastructure and Computational Biology, National Institute of Allergy and Infectious Diseases (131, 132).

LITERATURE CITED

1. Lecker SH, Goldberg AL, Mitch WE. 2006. Protein degradation by the ubiquitin-proteasome pathway in normal and disease states. *J. Am. Soc. Nephrol.* 17:1807–19
2. Komander D, Rape M. 2012. The ubiquitin code. *Annu. Rev. Biochem.* 81:203–29
3. Zheng N, Shabek N. 2017. Ubiquitin ligases: structure, function, and regulation. *Annu. Rev. Biochem.* 86:129–57
4. Morreale FE, Walden H. 2016. Types of ubiquitin ligases. *Cell* 165:248–48.e1
5. Petroski MD, Deshaies RJ. 2005. Function and regulation of cullin–RING ubiquitin ligases. *Nat. Rev. Mol. Cell Biol.* 6:9–20
6. Bulatov E, Ciulli A. 2015. Targeting cullin–RING E3 ubiquitin ligases for drug discovery: structure, assembly and small-molecule modulation. *Biochem. J.* 467:365–86
7. Lorenz S. 2018. Structural mechanisms of HECT-type ubiquitin ligases. *Biol. Chem.* 399:127–45
8. Weber J, Polo S, Maspero E. 2019. HECT E3 ligases: a tale with multiple facets. *Front. Physiol.* 10:370
9. Cotton TR, Lechtenberg BC. 2020. Chain reactions: molecular mechanisms of RBR ubiquitin ligases. *Biochem. Soc. Trans.* 48:1737–50
10. Haakonsen DL, Rape M. 2019. Branching out: improved signaling by heterotypic ubiquitin chains. *Trends Cell Biol.* 29:704–16
11. French ME, Koehler CF, Hunter T. 2021. Emerging functions of branched ubiquitin chains. *Cell Discov.* 7:6
12. Swatek KN, Komander D. 2016. Ubiquitin modifications. *Cell Res.* 26:399–422
13. Nalepa G, Rolfe M, Harper JW. 2006. Drug discovery in the ubiquitin-proteasome system. *Nat. Rev. Drug Discov.* 5:596–613
14. Wertz IE, Wang X. 2019. From discovery to bedside: targeting the ubiquitin system. *Cell Chem. Biol.* 26:156–77
15. Huang X, Dixit VM. 2016. Drugging the undruggables: exploring the ubiquitin system for drug development. *Cell Res.* 26:484–98
16. Bondeson DP, Crews CM. 2017. Targeted protein degradation by small molecules. *Annu. Rev. Pharmacol. Toxicol.* 57:107–23

17. Zhou P, Bogacki R, McReynolds L, Howley PM. 2000. Harnessing the ubiquitination machinery to target the degradation of specific cellular proteins. *Mol. Cell* 6:751–56
18. Sakamoto KM, Kim KB, Kumagai A, Mercurio F, Crews CM, Deshaies RJ. 2001. Protacs: chimeric molecules that target proteins to the Skp1–Cullin–F box complex for ubiquitination and degradation. *PNAS* 98:8554–59
19. Schneekloth JS Jr., Fonseca FN, Koldobskiy M, Mandal A, Deshaies R, et al. 2004. Chemical genetic control of protein levels: selective in vivo targeted degradation. *J. Am. Chem. Soc.* 126:3748–54
20. Winter GE, Buckley DL, Paulk J, Roberts JM, Souza A, et al. 2015. Phthalimide conjugation as a strategy for in vivo target protein degradation. *Science* 348:1376–81
21. Deshaies RJ. 2015. Protein degradation: prime time for PROTACs. *Nat. Chem. Biol.* 11:634–35
22. Bondeson DP, Mares A, Smith IE, Ko E, Campos S, et al. 2015. Catalytic in vivo protein knockdown by small-molecule PROTACs. *Nat. Chem. Biol.* 11:611–17
23. Lu J, Qian Y, Altieri M, Dong H, Wang J, et al. 2015. Hijacking the E3 ubiquitin ligase cereblon to efficiently target BRD4. *Chem Biol* 22:755–63
24. Zengerle M, Chan KH, Ciulli A. 2015. Selective small molecule induced degradation of the BET bromodomain protein BRD4. *ACS Chem. Biol.* 10:1770–77
25. Mullard A. 2021. Targeted protein degraders crowd into the clinic. *Nat. Rev. Drug Discov.* 20:247–50
26. Alabi SB, Crews CM. 2021. Major advances in targeted protein degradation: PROTACs, LYTACs, and MADTACs. *J. Biol. Chem.* 296:100647
27. Roth S, Fulcher LJ, Sapkota GP. 2019. Advances in targeted degradation of endogenous proteins. *Cell. Mol. Life Sci.* 76:2761–77
28. Harper JW, Schulman BA. 2021. Cullin-RING ubiquitin ligase regulatory circuits: a quarter century beyond the F-box hypothesis. *Annu. Rev. Biochem.* 90:403–29
29. Angers S, Thorpe CJ, Biechele TL, Goldenberg SJ, Zheng N, et al. 2006. The KLHL12–Cullin-3 ubiquitin ligase negatively regulates the Wnt–β-catenin pathway by targeting Dishevelled for degradation. *Nat. Cell Biol.* 8:348–57
30. Funato Y, Terabayashi T, Sakamoto R, Okuzaki D, Ichise H, et al. 2010. Nucleoredoxin sustains Wnt/β-catenin signaling by retaining a pool of inactive Dishevelled protein. *Curr. Biol.* 20:1945–52
31. Shami Shah A, Batrouni AG, Kim D, Punyala A, Cao W, et al. 2019. PLEKHA4/*kramer* attenuates Dishevelled ubiquitination to modulate Wnt and planar cell polarity signaling. *Cell Rep.* 27:2157–70.e8
32. Zhao B, Payne WG, Sai J, Lu Z, Olejniczak ET, Fesik SW. 2020. Structural elucidation of peptide binding to KLHL-12, a substrate specific adapter protein in a Cul3-Ring E3 ligase complex. *Biochemistry* 59:964–69
33. Chen Z, Wasney GA, Picaud S, Filippakopoulos P, Vedadi M, et al. 2020. Identification of a PGXPP degron motif in Dishevelled and structural basis for its binding to the E3 ligase KLHL12. *Open Biol.* 10:200041
34. de Brevern AG. 2016. Extension of the classical classification of β-turns. *Sci. Rep.* 6:33191
35. Chen Z, Picaud S, Filippakopoulos P, D'Angiolella V, Bullock AN. 2019. Structural basis for recruitment of DAPK1 to the KLHL20 E3 ligase. *Structure* 27:1395–404.e4
36. Zhuang M, Calabrese MF, Liu J, Waddell MB, Nourse A, et al. 2009. Structures of SPOP-substrate complexes: insights into molecular architectures of BTB-Cul3 ubiquitin ligases. *Mol. Cell* 36:39–50
37. Ostertag MS, Messias AC, Sattler M, Popowicz GM. 2019. The structure of the SPOP-Pdx1 interface reveals insights into the phosphorylation-dependent binding regulation. *Structure* 27:327–34.e3
38. Lumpkin RJ, Baker RW, Leschziner AE, Komives EA. 2020. Structure and dynamics of the ASB9 CUL–RING E3 ligase. *Nat. Commun.* 11:2866
39. Varshavsky A. 2019. N-degron and C-degron pathways of protein degradation. *PNAS* 116:358–66
40. Timms RT, Koren I. 2020. Tying up loose ends: the N-degron and C-degron pathways of protein degradation. *Biochem. Soc. Trans.* 48:1557–67
41. Santt O, Pfirrmann T, Braun B, Juretschke J, Kimmig P, et al. 2008. The yeast GID complex, a novel ubiquitin ligase (E3) involved in the regulation of carbohydrate metabolism. *Mol. Biol. Cell* 19:3323–33
42. Hammerle M, Bauer J, Rose M, Szallies A, Thumm M, et al. 1998. Proteins of newly isolated mutants and the amino-terminal proline are essential for ubiquitin-proteasome-catalyzed catabolite degradation of fructose-1,6-bisphosphatase of *Saccharomyces cerevisiae*. *J. Biol. Chem.* 273:25000–5

43. Chen SJ, Wu X, Wadas B, Oh JH, Varshavsky A. 2017. An N-end rule pathway that recognizes proline and destroys gluconeogenic enzymes. *Science* 355:eaal3655
44. Xiao Q, Zhang FR, Nacev BA, Liu JO, Pei DH. 2010. Protein N-terminal processing: substrate specificity of *Escherichia coli* and human methionine aminopeptidases. *Biochemistry* 49:5588–99
45. Dong C, Zhang H, Li L, Tempel W, Loppnau P, Min J. 2018. Molecular basis of GID4-mediated recognition of degrons for the Pro/N-end rule pathway. *Nat. Chem. Biol.* 14:466–73
46. Koren I, Timms RT, Kula T, Xu Q, Li MZ, Elledge SJ. 2018. The eukaryotic proteome is shaped by E3 ubiquitin ligases targeting C-terminal degrons. *Cell* 173:1622–35.e14
47. Rusnac DV, Lin HC, Canzani D, Tien KX, Hinds TR, et al. 2018. Recognition of the diglycine C-end degron by CRL2(KLHDC2) ubiquitin ligase. *Mol. Cell* 72:813–22.e4
48. Kershaw NJ, Murphy JM, Liau NP, Varghese LN, Laktyushin A, et al. 2013. SOCS3 binds specific receptor–JAK complexes to control cytokine signaling by direct kinase inhibition. *Nat. Struct. Mol. Biol.* 20:469–76
49. Liau NPD, Laktyushin A, Lucet IS, Murphy JM, Yao S, et al. 2018. The molecular basis of JAK/STAT inhibition by SOCS1. *Nat. Commun.* 9:1558
50. Zadjali F, Pike AC, Vesterlund M, Sun J, Wu C, et al. 2011. Structural basis for c-KIT inhibition by the suppressor of cytokine signaling 6 (SOCS6) ubiquitin ligase. *J. Biol. Chem.* 286:480–90
51. Kung WW, Ramachandran S, Makukhin N, Bruno E, Ciulli A. 2019. Structural insights into substrate recognition by the SOCS2 E3 ubiquitin ligase. *Nat. Commun.* 10:2534
52. Ivan M, Kondo K, Yang H, Kim W, Valiando J, et al. 2001. HIFα targeted for VHL-mediated destruction by proline hydroxylation: implications for O_2 sensing. *Science* 292:464–68
53. Jaakkola P, Mole DR, Tian YM, Wilson MI, Gielbert J, et al. 2001. Targeting of HIF-α to the von Hippel-Lindau ubiquitylation complex by O_2-regulated prolyl hydroxylation. *Science* 292:468–72
54. Min JH, Yang H, Ivan M, Gertler F, Kaelin WG Jr., Pavletich NP. 2002. Structure of an HIF-1α–pVHL complex: hydroxyproline recognition in signaling. *Science* 296:1886–89
55. Hon WC, Wilson MI, Harlos K, Claridge TD, Schofield CJ, et al. 2002. Structural basis for the recognition of hydroxyproline in HIF-1α by pVHL. *Nature* 417:975–78
56. Galdeano C, Gadd MS, Soares P, Scaffidi S, Van Molle I, et al. 2014. Structure-guided design and optimization of small molecules targeting the protein–protein interaction between the von Hippel–Lindau (VHL) E3 ubiquitin ligase and the hypoxia inducible factor (HIF) alpha subunit with in vitro nanomolar affinities. *J. Med. Chem.* 57:8657–63
57. Frost J, Galdeano C, Soares P, Gadd MS, Grzes KM, et al. 2016. Potent and selective chemical probe of hypoxic signalling downstream of HIF-α hydroxylation via VHL inhibition. *Nat. Commun.* 7:13312
58. Guo B, Phillips JD, Yu Y, Leibold EA. 1995. Iron regulates the intracellular degradation of iron regulatory protein 2 by the proteasome. *J. Biol. Chem.* 270:21645–51
59. Haile DJ, Rouault TA, Harford JB, Kennedy MC, Blondin GA, et al. 1992. Cellular regulation of the iron-responsive element binding protein: disassembly of the cubane iron-sulfur cluster results in high-affinity RNA binding. *PNAS* 89:11735–39
60. Hanson ES, Foot LM, Leibold EA. 1999. Hypoxia post-translationally activates iron-regulatory protein 2. *J. Biol. Chem.* 274:5047–52
61. Hanson ES, Rawlins ML, Leibold EA. 2003. Oxygen and iron regulation of iron regulatory protein 2. *J. Biol. Chem.* 278:40337–42
62. Iwai K, Klausner RD, Rouault TA. 1995. Requirements for iron-regulated degradation of the RNA binding protein, iron regulatory protein 2. *EMBO J.* 14:5350–57
63. Salahudeen AA, Thompson JW, Ruiz JC, Ma HW, Kinch LN, et al. 2009. An E3 ligase possessing an iron-responsive hemerythrin domain is a regulator of iron homeostasis. *Science* 326:722–26
64. Vashisht AA, Zumbrennen KB, Huang X, Powers DN, Durazo A, et al. 2009. Control of iron homeostasis by an iron-regulated ubiquitin ligase. *Science* 326:718–21
65. Wang H, Shi H, Rajan M, Canarie ER, Hong S, et al. 2020. FBXL5 regulates IRP2 stability in iron homeostasis via an oxygen-responsive [2Fe2S] cluster. *Mol. Cell* 78:31–41.e5
66. Thompson JW, Salahudeen AA, Chollangi S, Ruiz JC, Brautigam CA, et al. 2012. Structural and molecular characterization of iron-sensing hemerythrin-like domain within F-box and leucine-rich repeat protein 5 (FBXL5). *J. Biol. Chem.* 287:7357–65

67. Tan X, Calderon-Villalobos LI, Sharon M, Zheng C, Robinson CV, et al. 2007. Mechanism of auxin perception by the TIR1 ubiquitin ligase. *Nature* 446:640–45
68. Sheard LB, Tan X, Mao H, Withers J, Ben-Nissan G, et al. 2010. Jasmonate perception by inositol-phosphate-potentiated COI1-JAZ co-receptor. *Nature* 468:400–5
69. Che Y, Gilbert AM, Shanmugasundaram V, Noe MC. 2018. Inducing protein–protein interactions with molecular glues. *Bioorg. Med. Chem. Lett.* 28:2585–92
70. Schreiber SL. 2021. The rise of molecular glues. *Cell* 184:3–9
71. Vargesson N. 2015. Thalidomide-induced teratogenesis: history and mechanisms. *Birth Defects Res. C Embryo Today* 105:140–56
72. Ito T, Ando H, Suzuki T, Ogura T, Hotta K, et al. 2010. Identification of a primary target of thalidomide teratogenicity. *Science* 327:1345–50
73. Chamberlain PP, Lopez-Girona A, Miller K, Carmel G, Pagarigan B, et al. 2014. Structure of the human Cereblon–DDB1–lenalidomide complex reveals basis for responsiveness to thalidomide analogs. *Nat. Struct. Mol. Biol.* 21:803–9
74. Fischer ES, Bohm K, Lydeard JR, Yang H, Stadler MB, et al. 2014. Structure of the DDB1–CRBN E3 ubiquitin ligase in complex with thalidomide. *Nature* 512:49–53
75. Lu G, Middleton RE, Sun H, Naniong M, Ott CJ, et al. 2014. The myeloma drug lenalidomide promotes the cereblon-dependent destruction of Ikaros proteins. *Science* 343:305–9
76. Kronke J, Udeshi ND, Narla A, Grauman P, Hurst SN, et al. 2014. Lenalidomide causes selective degradation of IKZF1 and IKZF3 in multiple myeloma cells. *Science* 343:301–5
77. Matyskiela ME, Clayton T, Zheng X, Mayne C, Tran E, et al. 2020. Crystal structure of the SALL4–pomalidomide–cereblon–DDB1 complex. *Nat. Struct. Mol. Biol.* 27:319–22
78. Sievers QL, Petzold G, Bunker RD, Renneville A, Slabicki M, et al. 2018. Defining the human C2H2 zinc finger degrome targeted by thalidomide analogs through CRBN. *Science* 362:eaat0572
79. Uehara T, Minoshima Y, Sagane K, Sugi NH, Mitsuhashi KO, et al. 2017. Selective degradation of splicing factor CAPERα by anticancer sulfonamides. *Nat. Chem. Biol.* 13:675–80
80. Han T, Goralski M, Gaskill N, Capota E, Kim J, et al. 2017. Anticancer sulfonamides target splicing by inducing RBM39 degradation via recruitment to DCAF15. *Science* 356:eaal3755
81. Du X, Volkov OA, Czerwinski RM, Tan H, Huerta C, et al. 2019. Structural basis and kinetic pathway of RBM39 recruitment to DCAF15 by a sulfonamide molecular glue E7820. *Structure* 27:1625–33.e3
82. Faust TB, Yoon H, Nowak RP, Donovan KA, Li Z, et al. 2020. Structural complementarity facilitates E7820-mediated degradation of RBM39 by DCAF15. *Nat. Chem. Biol.* 16:7–14
83. Bussiere DE, Xie L, Srinivas H, Shu W, Burke A, et al. 2020. Structural basis of indisulam-mediated RBM39 recruitment to DCAF15 E3 ligase complex. *Nat. Chem. Biol.* 16:15–23
84. Protein Data Bank in Europe, European Bioinformatics Institute. 2022. PDBePISA (protein interfaces, surfaces and assemblies). *Interactive tool*. **http://www.ebi.ac.uk/pdbe/prot_int/pistart.html**
85. Krissinel E, Henrick K. 2007. Inference of macromolecular assemblies from crystalline state. *J. Mol. Biol.* 372:774–97
86. Aberle H, Bauer A, Stappert J, Kispert A, Kemler R. 1997. β-catenin is a target for the ubiquitin-proteasome pathway. *EMBO J.* 16:3797–804
87. Kitagawa M, Hatakeyama S, Shirane M, Matsumoto M, Ishida N, et al. 1999. An F-box protein, FWD1, mediates ubiquitin-dependent proteolysis of β-catenin. *EMBO J.* 18:2401–10
88. Rubinfeld B, Robbins P, El-Gamil M, Albert I, Porfiri E, Polakis P. 1997. Stabilization of β-catenin by genetic defects in melanoma cell lines. *Science* 275:1790–92
89. Polakis P. 2012. Wnt signaling in cancer. *Cold Spring Harb. Perspect. Biol.* 4:a008052
90. Simonetta KR, Taygerly J, Boyle K, Basham SE, Padovani C, et al. 2019. Prospective discovery of small molecule enhancers of an E3 ligase-substrate interaction. *Nat. Commun.* 10:1402
91. Slabicki M, Kozicka Z, Petzold G, Li YD, Manojkumar M, et al. 2020. The CDK inhibitor CR8 acts as a molecular glue degrader that depletes cyclin K. *Nature* 585:293–97
92. Mayor-Ruiz C, Bauer S, Brand M, Kozicka Z, Siklos M, et al. 2020. Rational discovery of molecular glue degraders via scalable chemical profiling. *Nat. Chem. Biol.* 16:1199–207
93. Lv L, Chen P, Cao L, Li Y, Zeng Z, et al. 2020. Discovery of a molecular glue promoting CDK12-DDB1 interaction to trigger cyclin K degradation. *eLife* 9:e59994

94. Slabicki M, Yoon H, Koeppel J, Nitsch L, Roy Burman SS, et al. 2020. Small-molecule-induced polymerization triggers degradation of BCL6. *Nature* 588:164–68
95. Pettersson M, Crews CM. 2019. Proteolysis targeting chimeras (PROTACs)—past, present and future. *Drug Discov. Today Technol.* 31:15–27
96. Sun X, Gao H, Yang Y, He M, Wu Y, et al. 2019. PROTACs: great opportunities for academia and industry. *Signal Transduct. Target. Ther.* 4:64
97. Verma R, Mohl D, Deshaies RJ. 2020. Harnessing the power of proteolysis for targeted protein inactivation. *Mol. Cell* 77:446–60
98. Ishida T, Ciulli A. 2021. E3 ligase ligands for PROTACs: how they were found and how to discover new ones. *SLAS Discov.* 26:484–502
99. Gadd MS, Testa A, Lucas X, Chan KH, Chen W, et al. 2017. Structural basis of PROTAC cooperative recognition for selective protein degradation. *Nat. Chem. Biol.* 13:514–21
100. Roy MJ, Winkler S, Hughes SJ, Whitworth C, Galant M, et al. 2019. SPR-measured dissociation kinetics of PROTAC ternary complexes influence target degradation rate. *ACS Chem. Biol.* 14:361–68
101. Bondeson DP, Smith BE, Burslem GM, Buhimschi AD, Hines J, et al. 2018. Lessons in PROTAC design from selective degradation with a promiscuous warhead. *Cell Chem. Biol.* 25:78–87.e5
102. Baratta MG, Schinzel AC, Zwang Y, Bandopadhayay P, Bowman-Colin C, et al. 2015. An in-tumor genetic screen reveals that the BET bromodomain protein, BRD4, is a potential therapeutic target in ovarian carcinoma. *PNAS* 112:232–37
103. Fujisawa T, Filippakopoulos P. 2017. Functions of bromodomain-containing proteins and their roles in homeostasis and cancer. *Nat. Rev. Mol. Cell Biol.* 18:246–62
104. Testa A, Hughes SJ, Lucas X, Wright JE, Ciulli A. 2020. Structure-based design of a macrocyclic PROTAC. *Angew. Chem. Int. Ed Engl.* 59:1727–34
105. Farnaby W, Koegl M, Roy MJ, Whitworth C, Diers E, et al. 2019. BAF complex vulnerabilities in cancer demonstrated via structure-based PROTAC design. *Nat. Chem. Biol.* 15:672–80
106. Sutherell CL, Tallant C, Monteiro OP, Yapp C, Fuchs JE, et al. 2016. Identification and development of 2,3-dihydropyrrolo[1,2-*a*]quinazolin-5(1*H*)-one inhibitors targeting bromodomains within the switch/sucrose nonfermenting complex. *J. Med. Chem.* 59:5095–101
107. Myrianthopoulos V, Gaboriaud-Kolar N, Tallant C, Hall ML, Grigoriou S, et al. 2016. Discovery and optimization of a selective ligand for the switch/sucrose nonfermenting-related bromodomains of polybromo protein-1 by the use of virtual screening and hydration analysis. *J. Med. Chem.* 59:8787–803
108. Soares P, Gadd MS, Frost J, Galdeano C, Ellis L, et al. 2018. Group-based optimization of potent and cell-active inhibitors of the von Hippel-Lindau (VHL) E3 ubiquitin ligase: structure-activity relationships leading to the chemical probe (2*S*,4*R*)-1-((*S*)-2-(1-cyanocyclopropanecarboxamido)-3,3-dimethylbutanoyl)-4-hydroxy-*N*-(4-(4-methylthiazol-5-yl)benzyl)pyrrolidine-2-carboxamide (VH298). *J. Med. Chem.* 61:599–618
109. Chan KH, Zengerle M, Testa A, Ciulli A. 2018. Impact of target warhead and linkage vector on inducing protein degradation: comparison of bromodomain and extra-terminal (BET) degraders derived from triazolodiazepine (JQ1) and tetrahydroquinoline (I-BET726) BET inhibitor scaffolds. *J. Med. Chem.* 61:504–13
110. Nowak RP, DeAngelo SL, Buckley D, He Z, Donovan KA, et al. 2018. Plasticity in binding confers selectivity in ligand-induced protein degradation. *Nat. Chem. Biol.* 14:706–14
111. Douglass EF Jr., Miller CJ, Sparer G, Shapiro H, Spiegel DA. 2013. A comprehensive mathematical model for three-body binding equilibria. *J. Am. Chem. Soc.* 135:6092–99
112. Chung CW, Dai H, Fernandez E, Tinworth CP, Churcher I, et al. 2020. Structural insights into PROTAC-mediated degradation of Bcl-xL. *ACS Chem. Biol.* 15:2316–23
113. Adams JM, Cory S. 2018. The BCL-2 arbiters of apoptosis and their growing role as cancer targets. *Cell Death Differ.* 25:27–36
114. Perini GF, Ribeiro GN, Pinto Neto JV, Campos LT, Hamerschlak N. 2018. BCL-2 as therapeutic target for hematological malignancies. *J. Hematol. Oncol.* 11:65
115. Mason KD, Carpinelli MR, Fletcher JI, Collinge JE, Hilton AA, et al. 2007. Programmed anuclear cell death delimits platelet life span. *Cell* 128:1173–86

116. He Y, Koch R, Budamagunta V, Zhang P, Zhang X, et al. 2020. DT2216—a Bcl-xL-specific degrader is highly active against Bcl-xL-dependent T cell lymphomas. *J. Hematol. Oncol.* 13:95
117. Tao ZF, Hasvold L, Wang L, Wang X, Petros AM, et al. 2014. Discovery of a potent and selective BCL-X_L inhibitor with in vivo activity. *ACS Med. Chem. Lett.* 5:1088–93
118. Dragovich PS, Pillow TH, Blake RA, Sadowsky JD, Adaligil E, et al. 2021. Antibody-mediated delivery of chimeric BRD4 degraders. Part 1: Exploration of antibody linker, payload loading, and payload molecular properties. *J. Med. Chem.* 64:2534–75
119. Dragovich PS, Pillow TH, Blake RA, Sadowsky JD, Adaligil E, et al. 2021. Antibody-mediated delivery of chimeric BRD4 degraders. Part 2: Improvement of in vitro antiproliferation activity and in vivo antitumor efficacy. *J. Med. Chem.* 64:2576–607
120. Law RP, Nunes J, Chung CW, Bantscheff M, Buda K, et al. 2021. Discovery and characterisation of highly cooperative FAK-degrading PROTACs. *Angew. Chem. Int. Ed Engl.* 60:23327–34
121. Sulzmaier FJ, Jean C, Schlaepfer DD. 2014. FAK in cancer: mechanistic findings and clinical applications. *Nat. Rev. Cancer* 14:598–610
122. Golubovskaya VM, Kweh FA, Cance WG. 2009. Focal adhesion kinase and cancer. *Histol. Histopathol.* 24:503–10
123. Cromm PM, Samarasinghe KTG, Hines J, Crews CM. 2018. Addressing kinase-independent functions of Fak via PROTAC-mediated degradation. *J. Am. Chem. Soc.* 140:17019–26
124. Popow J, Arnhof H, Bader G, Berger H, Ciulli A, et al. 2019. Highly selective PTK2 proteolysis targeting chimeras to probe focal adhesion kinase scaffolding functions. *J. Med. Chem.* 62:2508–20
125. Gao HY, Wu Y, Sun YH, Yang YQ, Zhou GB, Rao Y. 2020. Design, synthesis, and evaluation of highly potent FAK-targeting PROTACs. *ACS Med. Chem. Lett.* 11:1855–62
126. Kargbo RB. 2020. Chemically induced degradation of FAK–ALK for application in cancer therapeutics. *ACS Med. Chem. Lett.* 11:1367–68
127. Kargbo RB. 2020. Bifunctional pyrimidines as modulators of focal adhesion kinase. *ACS Med. Chem. Lett.* 11:409–11
128. Gao HY, Zheng CW, Du J, Wu Y, Sun YH, et al. 2020. FAK-targeting PROTAC as a chemical tool for the investigation of non-enzymatic FAK function in mice. *Protein Cell* 11:534–39
129. Tanjoni I, Walsh C, Uryu S, Tomar A, Nam JO, et al. 2010. PND-1186 FAK inhibitor selectively promotes tumor cell apoptosis in three-dimensional environments. *Cancer Biol. Ther.* 9:764–77
130. Raina K, Lu J, Qian Y, Altieri M, Gordon D, et al. 2016. PROTAC-induced BET protein degradation as a therapy for castration-resistant prostate cancer. *PNAS* 113:7124–29
131. Goddard TD, Huang CC, Meng EC, Pettersen EF, Couch GS, et al. 2017. UCSF ChimeraX: meeting modern challenges in visualization and analysis. *Protein Sci.* 27:14–25
132. Pettersen EF, Goddard TD, Huang CC, Meng EC, Couch GS, et al. 2021. UCSF ChimeraX: structure visualization for researchers, educators, and developers. *Protein Sci.* 30:70–82